

PbZr_{1-x}Ti_xO₃ by soft synthesis: Structural aspects

Swapan Kumar Pradhan,^{1,*} Milen Gateshki,¹ Markus Niederberger,^{2,3} Yang Ren,⁴ and Valeri Petkov^{1,†}

¹*Department of Physics, Central Michigan University, Mt. Pleasant, Michigan 48859, USA*

²*Colloid Chemistry, Max Planck Institute of Colloids and Interfaces, Research Campus Golm, 14424 Potsdam, Germany*

³*Department of Materials, ETH Zurich, Wolfgang-Pauli-Strasse 10, 8093 Zurich, Switzerland*

⁴*Advanced Photon Source, Argonne National Laboratory, Argonne, Illinois 60439, USA*

(Received 4 February 2007; revised manuscript received 19 April 2007; published 25 July 2007)

The structural aspects of a soft synthetic route employed to obtain fine crystallite PbZr_{1-x}Ti_xO₃ ($x=0,0.5,1$) powders are revealed by total x-ray diffraction and atomic pair distribution function analysis. It is found that the atomic-scale structure of the intermediate, highly disordered phase the route passes through resembles but is not exactly of the targeted, perovskite-type structure. It is suggested that future synthesis efforts are directed toward closing the observed “structure gap” as much as possible.

DOI: [10.1103/PhysRevB.76.014114](https://doi.org/10.1103/PhysRevB.76.014114)

PACS number(s): 61.10.Nz, 81.07.Bc

I. INTRODUCTION

Thanks to their high ferroelectric Curie temperature and piezoelectric response mixed crystalline PbZr_{1-x}Ti_xO₃ oxides with the perovskite structure are widely used in applications such as ultrasonic transducers, actuators, filters, resonators and detectors.¹⁻⁶ Usually they are obtained by a solid-state reaction of the pure metal (Pb, Zr, and Ti) oxides, hydroxides, or carbonates at temperatures between 873 K (Ti rich) and 1373 K (Zr rich oxides). Thus obtained crystalline powders, however, are coarse grains (~microns) and often are not quite homogeneous due to the volatility of lead oxide at high temperatures, limiting the usefulness of PZT in important industrial applications such as thin piezoelectric films, for example. This has spurred a search for alternative synthesis routes that are capable of yielding finer and more phase-pure PbZr_{1-x}Ti_xO₃ powders. Good progress has been made by employing soft synthesis methods based on sol-gel chemistry,⁷⁻¹⁰ coprecipitation,^{11,12} and thermal decomposition of polymeric-type precursors.¹³⁻¹⁶ Within this effort a nonaqueous sol-gel route has been developed recently that yields very homogeneous and fine (~10–30 nm) powders,⁷ allowing one to produce thin films with a mean surface roughness of the order of 0.13 nm only. The route involves mixing of standard chemicals followed by a solvothermal treatment at 473 K. First it yields a highly disordered (hereafter called precursor) phase which, when extra treated at 700–900 K, is then transformed into fine crystallite powders with the perovskite structure. Further lowering the crystallization temperature of the precursor phase would be advantageous since thin perovskite films are usually deposited on silicon substrates that tend to get damaged when exposed to temperature approaching 800 K. Good knowledge of the disorder- (precursor phase) order (fine perovskite crystallites) structural transformation would definitely help gain control over it. However, while the structure type of the synthesis route final products, crystalline PbZr_{1-x}Ti_xO₃ powders, is relatively easy to identify, that of the intermediate precursor phase is not. The problem stems from the fact that the atomic arrangement in highly disordered materials is difficult to study by traditional techniques for structure determination such as Bragg x-ray diffraction (XRD). Here we apply total

XRD coupled to atomic Pair Distribution Function (PDF) analysis^{17,18} to determine the atomic-scale structure of precursor phase. We find that it bares similarities to but yet is distinctly different from the perovskite-type structure and, furthermore, evolves substantially with Ti/Zr content. The results of our structure study suggest that soft synthesis routes may be made more friendly to technology if the intermediate stage/phase they usually go through is tailored to be as similar structurally to the perovskite-type phase as possible, since this would inevitably reduce the extra energy barrier (i.e., extra thermal treatment) needed for their completion.

II. EXPERIMENT

A. Sample preparation

Lead (II) acetylacetonate [CH₃COCH=C(O)CH₃]₂Pb, titanium isopropoxide Ti[OCH(CH₃)₂]₄, zirconium isopropoxide Zr[OCH(CH₃)₂]₄.HOCH(CH₃)₂, and 2-butanone, all obtained from Aldrich, were used. Three members of PbZr_{1-x}Ti_xO₃ family, with $x=0, 0.5$, and 1, were synthesized. The sample with $x=0.5$ is close to the so-called morphotropic composition known to exhibit the best piezoelectric properties. The end members PbTiO₃ (PT) and PbZrO₃ (PZ) were synthesized by mixing 1.23 mmol of titanium isopropoxide or zirconium isopropoxide isopropanal complex, respectively, with 2-butanone. Pb(Zr_{0.5}Ti_{0.5})O₃ oxide (PZT) was synthesized when both 0.58 mmol of Ti(OiPr)₄ and 0.65 mmol of Zr(OiPr)₄.iPrOH were used. All solutions were kept sealed at 473 K in Parr autoclaves for 24 h, then centrifuged. The extracted precipitates were washed with ethanol and dried in vacuum. The resulted heavily disordered (precursor) materials were transformed into crystalline PT, PZT, and PZ perovskites by extra thermal treatment at 673, 723, and 873 K, respectively, carried out for 4–6 h, in air. As TEM studies showed thus obtained crystalline powders were very fine, with an average crystallite size of 10–30 nm. More details of the preparation procedure can be found in Ref. 7.

B. X-ray diffraction experiments

The three precursor phases (marked with **p** in all plots) and the products of their crystallization (marked with **c** in all

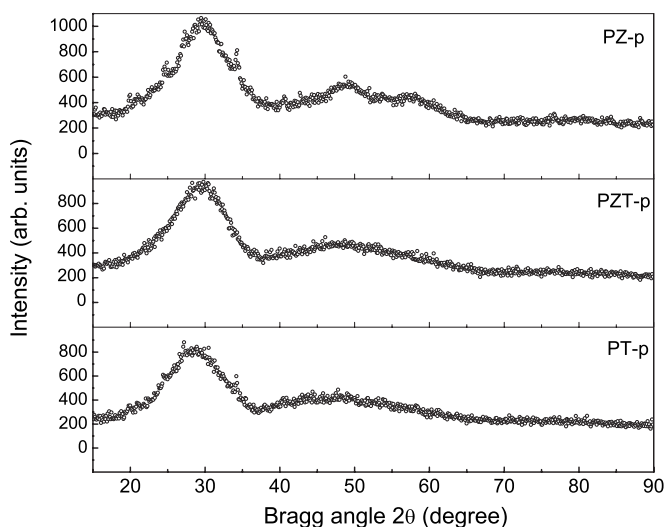


FIG. 1. Conventional ($\text{CuK}\alpha$ radiation) XRD patterns for the highly disordered precursors phases.

plots) were subjected to x-ray diffraction (XRD), at first using $\text{CuK}\alpha$ radiation (x-ray energy ~ 8 keV). Experimental XRD patterns are shown in Figs. 1 and 2, respectively. All samples were also subjected to XRD experiments at the beamline 11-ID-C (Advanced Photon Source, Argonne National Laboratory) using synchrotron radiation of energy 115.227 keV ($\lambda=0.1076$ Å). Synchrotron radiation x rays were employed for two reasons: First, the higher flux of synchrotron radiation x rays allowed us to measure the rather diffuse XRD pattern of the precursor phases with a greatly improved statistical accuracy. Second, the higher energy of synchrotron radiation x-rays allowed to collect data over a much wider range ($1-30$ Å $^{-1}$) of scattering vectors Q . Both are important¹⁸ for the success of the atomic PDF analysis

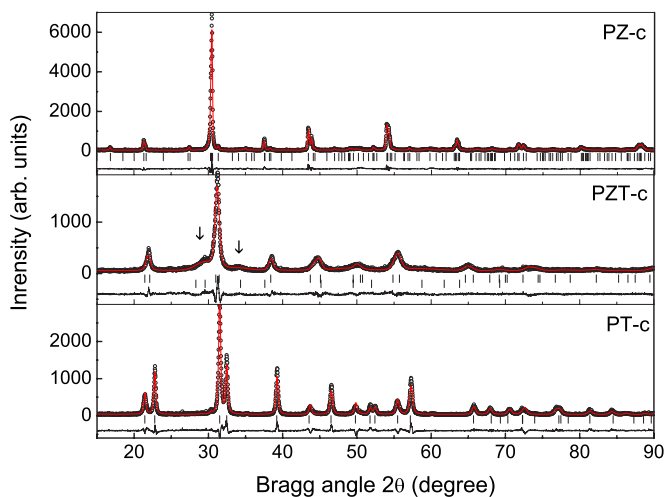


FIG. 2. (Color online) Conventional ($\text{CuK}\alpha$ radiation; symbols) XRD patterns for PT, PZT, and PZ fine crystallite powders. Results from Rietveld analyses (full line) are presented as well. Difference (experimental minus computed data) curves and the positions of the Bragg peaks of the respective phases (see the text) are shown at the bottom of each plot. Arrows mark the weak diffraction features of the minority pyrochlore-type phase in PZT.

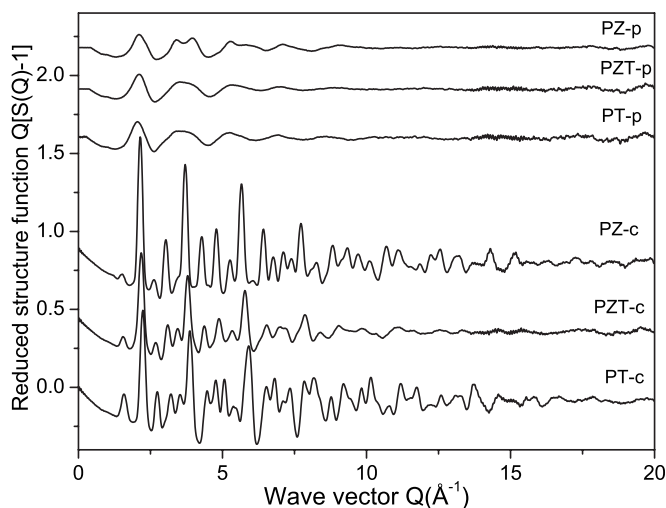


FIG. 3. Reduced structure functions (based on synchrotron radiation x-ray data) of the precursor phases (p) and the products of their crystallization (c).

employed here. Scattered synchrotron radiation was collected with an imaging plate detector (mar345). Up to ten images were taken from each of the samples. The corresponding images/scans were combined, subjected to geometrical corrections, integrated, reduced to one-dimensional XRD patterns, converted into absolute (electron) units and reduced to the so-called structure functions.¹⁸⁻²¹ Experimental structure functions are shown in Fig. 3. All processing of the synchrotron XRD data was done with the help of the program RAD.¹²

III. RESULTS

As can be seen in Fig. 1 the XRD patterns of PT, PZT, and PZ precursor phases are very diffuse, as usually found with highly disordered materials. Such XRD patterns are very difficult, if not impossible, to analyze employing traditional techniques for structure determination such as Rietveld analysis.^{22,23} Understandably all attempts to fit the experimental data, as they are, with models based on the perovskite-type structure and several other structure types found in the $\text{PbZr}_{1-x}\text{Ti}_x\text{O}_3$ family, failed. The reason is that Rietveld analysis relies on sharp diffraction features that are, as a rule (see Fig. 1), not exhibited by the XRD patterns of highly disordered materials. In contrast, the XRD patterns of crystalline PT, PZT, and PZ powders obtained from the precursor phases (see Fig. 2) are rich in sharp diffraction features (Bragg peaks) and may be analyzed easily in the traditional (e.g., Rietveld) way. Such analyses were carried out²⁴ and the XRD patterns of PT- c and PZ- c oxides were very well reproduced by a model based on the perovskite structure with tetragonal ($P4mm$) and orthorhombic ($Pbam$) symmetry, respectively. The XRD pattern of PZT- c was well reproduced by a model based on a major ($\sim 80\%$) perovskite-type ($P4mm$) and a minor ($\sim 20\%$) pyrochlore-type ($Fd-3m$) phases. Fragments from the technologically important perovskite-type structure are shown in Fig. 4. Results from

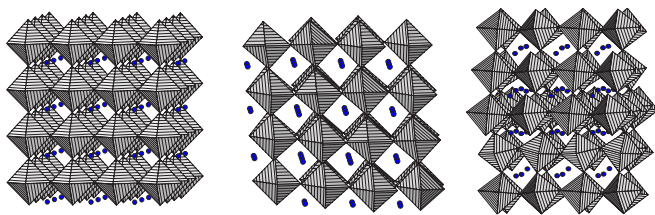


FIG. 4. (Color online) Fragments from the perovskite-type structure occurring in crystalline PbZr_{1-x}Ti_xO₃ at room temperature. The structure may be viewed as a 3D network of (Ti/Zr)O₆ octahedra with Pb atoms (circles) filling up the network cavities. The network is of tetragonal ($x=0$ to ~ 0.45 , left), rhombohedral ($0.45 < x < 0.99$, middle), and orthorhombic ($x \sim 1$, right) symmetry.

the Rietveld analyses are summarized in Tables I and II. Inspection of the tables confirm that the soft synthesis route of Garnweitner *et al.*⁷ is capable of yielding perovskite-type PbZr_{1-x}Ti_xO₃ ($x=0, 0.5, 1$) fine crystallite powders at temperatures that are considerably lower than those employed in the traditional solid-state synthesis. The structural inhomogeneity observed with PZT-*c* is not a surprise. PbZr_{1-x}Ti_xO₃ materials with a composition close to the morphotropic boundary ($x \sim 0.5$) are often reported to be either a two-phase mixture^{25–28} and/or to exhibit local monoclinic-type distortions,^{29–33} with the relative abundance of the two phases and/or the degree of monoclinic distortions are found to vary with the preparation conditions. However, the structural aspects of the route, in particular those of the transfor-

mation of the intermediate precursor phase into fine perovskite crystallites, are yet to be revealed. To achieve it we had to consider the total synchrotron XRD patterns in terms of the corresponding atomic PDFs, an approach that has proven recently to be very successful in structure studies of heavily disordered materials, including oxides.^{34–37} A comparison between the data of Figs. 1–3 exemplifies the different way the same diffraction features appear, and hence, are accounted for in structure studies relying on conventional (CuK α) XRD patterns and on total (high-energy synchrotron x rays) XRD data converted to structure factors/PDFs. Conventional XRD patterns are dominated by strong and sharp, if any, diffraction features at lower Bragg angles (wave vectors; see Figs. 1 and 2 and are thus mostly sensitive to longer-range, periodic atomic ordering in materials. All diffraction features, including sharp peaks as well as diffuselike oscillations, appear almost equally strong in structure factors $Q[S(Q)-1]$ extracted from total XRD patterns (see Fig. 3) and are thus accounted for in PDF studies. This enhances the sensitivity of the latter to local (shorter-range) atomic ordering rendering the PDF approach very well suited to study materials with substantial structural disorder. Furthermore, thanks to the properties of Fourier transformation^{18,38} the slow oscillating (diffuselike scattering) components of the total XRD data appear as sharp and, hence, easily identified PDF features in real space. Last but not the least, atomic PDFs reflect total XRD data corrected for all experimental artifacts and, thus, directly give relative positions of atoms enabling convenient testing and refinement of structural models, as demonstrated below. Experimental atomic PDFs $G(r)=4\pi r[\rho(r)-\rho_0]$, where $\rho(r)$ and ρ_0 are the local and

TABLE I. Parameters of the lattices of three highly disordered precursor (marked with *p*) and crystalline (marked with *c*) PbZr_{1-x}Ti_xO₃, with $x=1$ (PT), $x=0.5$ (PZT), and $x=0$ (PZ) phases, as obtained through Rietveld and PDF analyses. The crystallographic symmetry of the lattices is tetragonal (for the PT-*c/p* and the major PZT-*c/p* phases), orthorhombic (for the PZ-*p* phase), and cubic (for the minor PZT-*p* and the PZ-*p* phases). The small differences between the lattice parameters resulted from the Rietveld and PDF analyses are due to the fact that the XRD pattern and atomic PDF are not the same experimental quantity with the latter is much more sensitive to the local atomic ordering than the former. Literature data are also reported for comparison.

Phase	Lattice parameters (Å)		
	Rietveld	PDF	Literature data/ Reference
PT- <i>c</i>	$a=3.9035$ $c=4.1447$	$a=3.9068(3)$ $c=4.1415(7)$	$a=3.902$ $c=4.156$ (Ref. 44)
PT- <i>p</i>		$a=4.060(3)$ $c=5.010(7)$	$a=3.9665$ $c=4.9831$ (Ref. 47).
PZT- <i>c</i> major	$a=4.0432$ $c=4.1013$	$a=4.0490(7)$ $c=4.1054(4)$	$a=4.0303$ $c=4.1449$ (Ref. 56)
minor PZT- <i>p</i>	$a=10.5510$	$a=10.4312$ $a=3.997(4)$ $c=4.886(8)$	$a=10.4109$ (Ref. 57) $a=3.9665$ $c=4.9831$ (Ref. 47)
PZ- <i>c</i>	$a=5.8794$ $b=11.7795$ $c=8.2486$	$a=5.8811(12)$ $b=11.7970(11)$ $c=8.2629(19)$	$a=5.8741$ $b=11.7759$ $c=8.1969$ (Ref. 58)
PZ- <i>p</i>		$a=10.551(8)$	$a=10.6349$ (Ref. 57).

TABLE II. Positions of atoms within the unit cells of the lattices reported in Table I. Literature data are also reported for comparison. Again, the differences between the structure parameters resulted from the Rietveld and PDF analyses may be explained with the fact that the XRD pattern and atomic PDF are not the same experimental quantity with the latter is much more sensitive to the local atomic ordering than the former.

Phase	Atomic coordinates/Rietv.			Atomic coordinates/PDF			Literature data/references			Goodness of fit ^a σ R_{wp} ^a				
	atom	x	y	z	atom	x	y	z	atom	x	y	z		
PT- <i>c</i>	Ti			0.510	Ti			0.510	Ti			0.537	1.76	16.7%
	O1			0.255	O1			0.133	O1			0.11		
	O2			0.646	O2			0.631	O2			0.617 (Ref. 44)		
PT- <i>p</i>					Pb			0.238	Pb			0.239		
					Ti			0.158	Ti			0.126		
					O			0.598	O			0.483 (Ref. 47)		
PZT- <i>c</i> major	Pb			0.052	Pb			0.032	Pb			0.024	1.56	14.6%
	Zr			0.529	Zr			0.565	Zr			0.564		
	Ti			0.529	Ti			0.565	Ti			0.564		
	O1			0.272	O1			0.091	O1			0.092		
	O2			0.628	O2			0.621	O2			0.611 (Ref. 56)		
minor	O	0.433			O	0.305			O	0.433				
PZT- <i>p</i>					Pb			0.238	Pb			0.239		
					Ti			0.086	Ti			0.126		
					O			0.580	O			0.483 (Ref. 47)		
PZ- <i>c</i>	Pb1	0.699	0.131		Pb1	0.700	0.126		Pb1	0.700	0.123		1.68	16.0%
	Pb2	0.725	0.122		Pb 2	0.709	0.129		Pb2	0.706	0.130			
	Zr	0.249	0.123	0.246	Zr	0.236	0.124	0.248	Zr	0.242	0.125	0.249		
	O1	0.283	0.133		O1	0.229	0.127		O1	0.275	0.155			
	O2	0.276	0.160		O2	0.376	-0.020		O2	0.300	0.096			
	O3	0.186	0.159	0.253	O3	0.055	0.268	0.280	O3	0.032	0.262	0.279		
	O4			0.241	O4			0.227	O4			0.203		
O5			0.196	O5			0.228	O5			0.229 (Ref. 58)			
PZ- <i>p</i>	O				O	0.383			O			0.433 (Ref. 57)		

^aRietveld analyses agreement factors are shown in the table only. the PDF analyses agreement factors are reported in Figs. 5–9.

average atomic number densities, respectively, and r is the radial distance are shown in Figs. 5 and 6. As can be seen in the figures, the experimental PDFs exhibit a series of well-defined peaks, each corresponding to a frequently occurring interatomic distance (i.e., a well-defined coordination sphere) in the respective material. Peaks in the PDFs for the precursor phases extend to distances of approximately 1.5 nm only, showing that those materials are heavily disordered but, locally, still exhibit a well-defined atomic structure. Peaks in the PDFs for the crystalline oxides persist to much longer interatomic distances reflecting the presence of an extended sequence of distinct coordination spheres in these long-range ordered materials.

As can be seen in Fig. 6 all important details in the experimental PDFs for the crystalline oxides can be very well reproduced by the structure models already attempted by traditional Rietveld analyses. The calculation of the model PDFs was done with the help of the program PDFFIT⁴⁰ using literature data for the corresponding structures. Structure pa-

rameters resulted by the PDF analyses are summarized in Tables I and II. Data presented in the tables show that Rietveld (relying only on the Bragg component of the XRD patterns) and PDF (relying on the total XRD patterns) analyses yield very similar estimates for the structural parameters of materials with good crystallinity. Also, both Rietveld (see Fig. 2) and PDF analyses (compare the data in Figs. 6 and 7) clearly reveal the presence of a second (minor) phase in crystalline PZT. Traditional studies, however, cannot handle properly the very diffuse XRD patterns of the highly disordered precursor phases. On the other hand, the PDFs of the precursor phases show several structure-relevant features and lend themselves to structure search and refinement. For example, the PDFs of the precursor phases show a first, low-amplitude peak centered at about 1.9–2.5 Å and a second, higher amplitude one at approximately 4 Å. Indeed those are the typical metal-oxygen and metal-metal distances, respectively, found in $\text{PbZr}_{1-x}\text{Ti}_x\text{O}_3$ oxides (metal = Ti/Zr/Pb). This indicated that the first metal-oxygen and

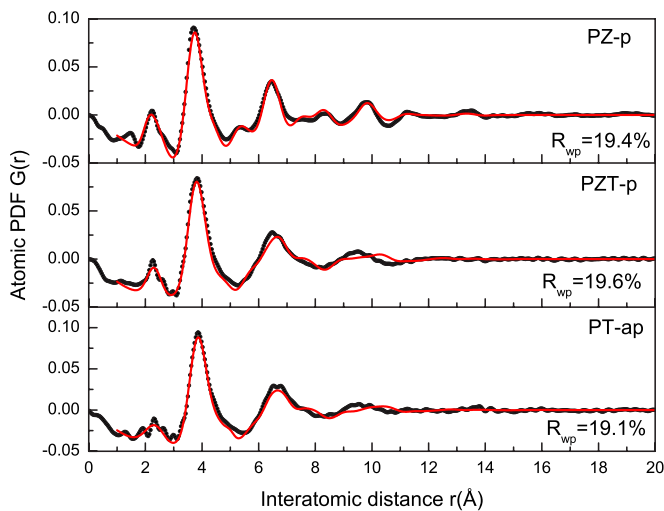


FIG. 5. (Color online) Experimental (symbols) and calculated (solid line) atomic PDFs for the precursor phases. The calculated data are based on the following model structures (see the text): PT-*p* on tetragonal $\text{Pb}_{1-x}(\text{TiO})_x\text{O}$, with $x=0.5$; PZT-*p* on tetragonal $[\text{Pb}_{1-x}(\text{Ti}_y, \text{Zr}_y)\text{O}]_x\text{O}$ with $x=0.5$ and $y=0.5$; and PZ-*p* on disordered cubic ($\text{Pb}_2\text{Zr}_2\text{O}_6$) pyrochlore. The agreement (model vs experiment) factors R_{wp} (Ref. 39), are reported as well.

metal-metal coordination spheres/units in the precursor phases are relatively well defined, and prompted us to narrow the structure search to models exhibiting such coordination spheres/units. Note, conventional XRD patterns alone (see Fig. 1) do not reveal this important structural feature of the precursor phases in such a straightforward way.

IV. DISCUSSION

Previous traditional XRD studies have concluded that the local atomic ordering in all precursor phases exhibits

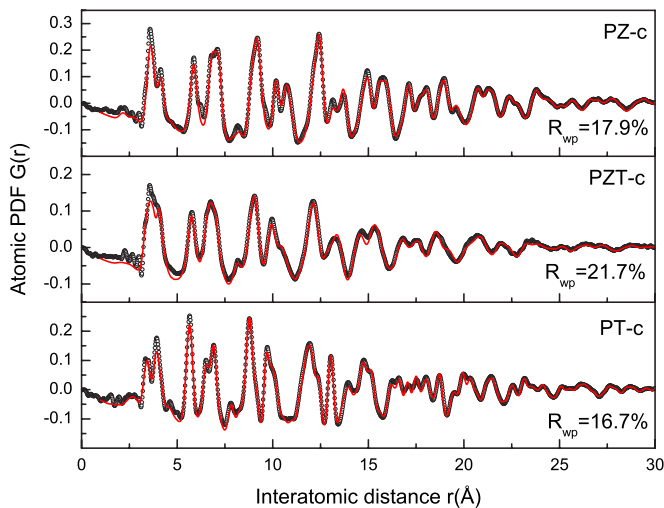


FIG. 6. (Color online) Experimental (symbols) and calculated (solid line) atomic PDFs for PT, PZT, and PZ fine crystallite powders. The calculated data are based on the following model structures: PT-*c* on tetragonal and PZ-*c* on orthorhombic perovskite (see Fig. 4), and PZT-*c* on a mixture of tetragonal perovskite and disordered cubic pyrochlore. The agreement (model vs experiment) factors R_{wp} are reported as well.

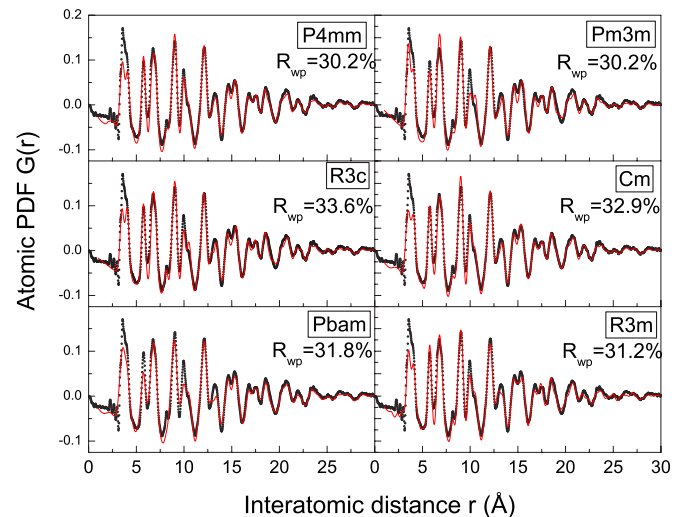


FIG. 7. (Color online) Experimental (symbols) and calculated (solid line) PDFs for crystalline PZT. The calculated data are based on models featuring single phases of different symmetry (indicated in the plot) all observed in Pb-Ti/Zr-O perovskites. The agreement (model vs experimental data) factors R_{wp} are reported as well. None of the single phase models can reproduce well the PDF peaks at approximately 4 and 10 Å while a two-phase model (see Fig. 6) can.

pyrochlore-type structural features.^{7,41} However, as our studies showed, the rather diffuse (i.e., featureless) XRD patterns of the precursor phases may also be reproduced by models based on other structure types, i.e., conventional XRD data do not provide a firm basis for an exact structure solution. To reveal the atomic-scale structure of the precursor phases unambiguously we tested a number of models, all with the Pb-Zr/Ti-O chemistry, and all based on structure types exhibiting first coordination spheres/units found in perovskites. The tests were conducted by computing model PDFs, using literature data (unit cell constants, atomic positions and rms atomic vibrations at room temperature) for the respective structures, and comparing the model data to the experimental PDFs of the precursor phases. The PT, PZT, and PZ stoichiometry was achieved by filling/emptying appropriate atomic positions in the model structures while strictly observing their symmetry/type. The very limited length of structural coherence in the precursor phases was modeled by multiplying the model PDF data with a decaying exponent as suggested in Ref. 42 and implemented in Ref. 43. The effect of the correction is to depress the PDF uniformly without changing its shape. These calculations were also done with the help of the program PDFFIT.⁴⁰ The PT precursor phase was approached first with a model based on the structure of the corresponding crystal tetragonal perovskite PbTiO_3 (*t*).⁴⁴ As can be seen in Fig. 8 the model reproduces the first neighbor metal-oxygen (PDF peak at $\sim 1.9\text{--}2.3$ Å) and metal-metal coordination (PDF peak ~ 4 Å) well but fails at longer interatomic distances (i.e., at higher coordination spheres), clearly showing that the atomic arrangement in the fine crystallite PbTiO_3 perovskite and its precursor is not quite the same. Other models, including one based on a hypothetical, highly disordered pyrochlore-type structure, performed bet-

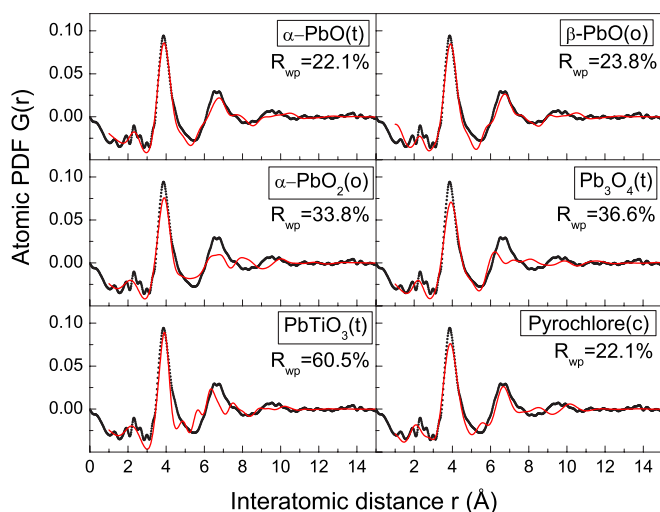


FIG. 8. (Color online) Experimental (symbols) and model (solid line) atomic PDFs for PT-*p*. The agreement factors (model vs experimental data) R_{wp} are reported as well. The fine structure of the first peak in the experimental PDF is due to data noise.

ter (see Fig. 8). A model based on the α -PbO-type structure,⁴⁵ namely, $Pb_{1-x}(TiO)_xO$ with $x=0.5$, however, outperformed all (see Fig. 5). Its parameters are listed in Tables I and II. The same set of structure models was also tested against the experimental PDF for the PZT precursor phase. Again, the best results were obtained with a model based on the α -PbO-type structure, namely, $[Pb_{1-x}(Ti_y, Zr_y)O]_xO$ with $x=0.5$ and $y=0.5$ (see Fig. 5). The parameters of the model structure are listed in Tables I and II. It may be noted that PbO-Ti/ZrO₂ solid solutions with the tetragonal structure of α -PbO-type have been observed in other studies as well.^{45–49} The structure of the PZ precursor phase was explored with a slightly different set of models to account for the different chemistry of Ti and Zr. Results from the tests are presented in Fig. 9. Here, again, the structure of the precursor phase was not possible to be approximated by that of the corresponding perovskite crystal, orthorhombic PbZrO₃. A highly disordered cubic, pyrochlore-type ($Pb_2Zr_2O_6$) structure,⁵⁰ with parameters listed in Tables I and II, performed best (see Fig. 5). This finding did not come as a surprise either since several other studies^{51–55} have reported the formation of a pyrochlore-type phase in low temperature processed, Zr-rich PZT powders. Fragments from the tetragonal $[Pb_{1-x}(Ti_y, Zr_y)O]_xO$ and cubic-pyrochlore $Pb_2Zr_2O_6$ structures are shown in Fig. 10.

In summary, the results of our structure study show that (i) metal and oxygen atoms in the precursor phases form relatively well-defined coordination spheres/units, (ii) that are correlated locally (~ 1.5 nm) only, (iii) yet, in contrast to completely disordered (amorphous) materials, form a distinct arrangement that may be described in terms of a few, crystallographic-type parameters (i.e., structure type, basic structural motif, repetitive/unit cell and local symmetry). (iv) In all three precursors that arrangement is of a network-type (v) and resembles, but does not correspond exactly to, the perovskite-type network found in the corresponding crystals. (vi) In particular, the Ti-rich precursor phase may be viewed

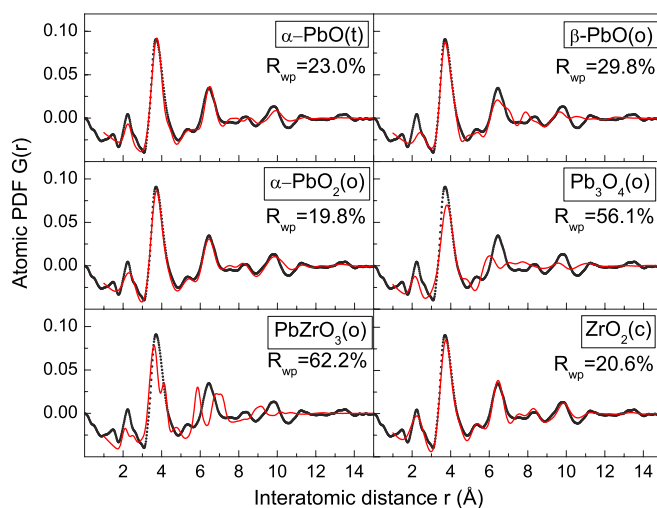


FIG. 9. (Color online) Experimental (symbols) and model (solid line) atomic PDFs for PZ-*p*. The agreement factors (model vs experimental data) R_{wp} are reported as well.

as a network of both edge and corner-sharing octahedral (Ti-O) units/sites with Pb atoms sitting in between them (see Fig. 9). Note, the corresponding perovskite crystal may be viewed as a network comprising only corner-sharing Ti-O₆ units (see Fig. 4). The Zr-rich the precursor phase may be viewed as a network of corner-sharing octahedral (Zr-O) units with Pb atoms sitting in between them. Note, this network does not stretch out in planes/columns as the one in the corresponding perovskite crystal (see Figs. 4 and 10). (vii) As such, the precursor phases would still need to overcome a substantial energy barrier to transform into crystalline perovskites (vii) but this transformation process (crystallization) may occur at temperature lower (700–900 K, as observed in practice) than that (900–1400 K) needed to complete a conventional solid-state syntheses. The reason is that key ingredients of the perovskite structure, octahedral-like (Ti/Zr-O) units/sites surrounding Pb atoms, are already present in the precursor phases. (ix) Also, since the coordination sequence/network coupling in Ti and Zr-rich precursors is significantly different (see Fig. 10), Ti and Zr may not mix well together

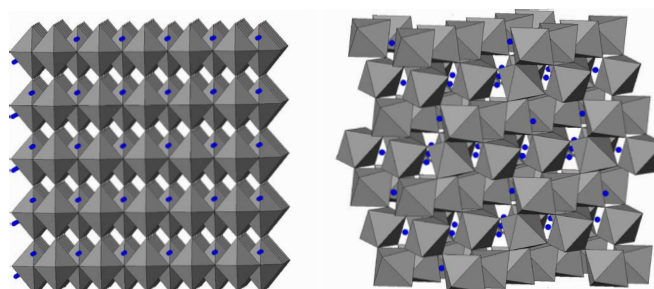


FIG. 10. (Color online) Fragments from the tetragonal $[Pb_{1-x}(Ti_y, Zr_y)O]_xO$ (α -PbO-type) and cubic $Pb_2Zr_2O_6$ (pyrochlore-type; O2 positions not shown) structures. Both structures comprise (Ti/Zr)-oxygen octahedral-like units assembled in a very (left) and not so (right) regular 3D network. Pb atoms (circles) occupy (partially) the network cavities.

at $x \sim 0.5$, resulting in a phase separation upon crystallization, as often observed in practice, (x) moreover, Ti- and Zr-rich precursors may need to overcome a significantly different energy barriers (PT needs extra heating at 723 K while PZ at 923 K, as observed in practice) to crystallize into perovskites.

An important outcome of our structure study is that it tips-off an approach to streamline further soft chemistry of very fine PZT powders. If the highly disordered precursor phase through which most soft synthesis routes go through is tailored to have the structure of perovskite, within the full length of structural coherence (~ 1.5 to 2 nm) it usually shows, the post-treatment/crystallization (i.e., the second step of the synthesis route) may then require lower, than currently needed, processing temperature to complete. This will definitely make soft synthesis methods even more attractive to PZT thin film industry.

V. CONCLUSION

Total x-ray diffraction and PDF data analysis can be very useful in elucidating the structural aspects of soft synthesis methods passing through heavily disordered intermediate phases such as those employed to obtain very fine PZT powders. The structural knowledge this non-traditional approach yields helps understand, explain, and predict the synthesis outcome and, hence, may help fabricate improved materials by intelligent design.

ACKNOWLEDGMENTS

The work was supported by NSF through Grant No. DMR 0304391(NIRT) and CMU through Grant No. REF C602281. Use of the Advanced Photon Source was supported by the U. S. Department of Energy, Office of Science, Office of Basic Energy Sciences, under Contract No. DE-AC02-06CH11357.

*On leave from Department of Physics, The University of Burdwan, Golapbag, Burdwan-713104, West Bengal, India.

†Author to whom correspondence should be addressed: petkov@phy.cmich.edu

¹Y. S. Hoon, S. H. Kim, S.-J. Lee, H. K. Kim, and M.-J. Lee, *Sens. Actuators, A* **125**, 463 (2006).

²M. Kobayashi, T. R. Olding, M. Sayer, and C.-K. Jen, *Ultrasonics* **39**, 675 (2002).

³J.-H. Kim, C.-D. Kim, M.-J. Kim, K.-L. Ha, and N. Chubachi, *Jpn. J. Appl. Phys., Part 1* **40**, 3652 (2001).

⁴M. Schreiter, R. Gabl, D. Pitzer, and W. Wersing, *J. Eur. Ceram. Soc.* **24**, 1589 (2004).

⁵T. Kawabata, M. Ikeda, M. Sakata, H. Goto, M. Matsumoto, and T. Yada, *Proc. Int. Conf. Solid-State Sensors and Actuators (Transducers '97)*, Chicago, IL, 1997 (IEEE, Chicago, 1997), Vol. 1, pp. 339–342.

⁶M. H. Kwak, S. E. Moon, S.-J. Lee, Y. T. Kim, H.-C. Ryu, and W.-J. Kim, *Integr. Ferroelectr.* **54**, 659 (2003).

⁷G. Garnweitner, J. Hentschel, M. Antonietti, and M. Neiderberger, *Chem. Mater.* **17**, 4594 (2005).

⁸J. Moon, J. A. Kerchner, H. Krarup, and J. H. Adair, *J. Mater. Res.* **14**, 425 (1999).

⁹Y. Deng, L. Liu, Y. Cheng, C. W. Nan, and S. J. Zhao, *Mater. Lett.* **57**, 1675 (2003).

¹⁰S. B. Cho, J. S. Noh, M. M. Leneka, and R. E. Riman, *J. Eur. Ceram. Soc.* **23**, 2323 (2003).

¹¹C. Liu, B. Zou, A. J. Rondinone, and Z. J. Zhang, *J. Am. Chem. Soc.* **123**, 4344 (2001).

¹²E. R. Camargo, M. Popa, J. Frantti, and M. Kakihana, *Chem. Mater.* **13**, 3943 (2001).

¹³T. K. Mandal and S. Ram, *Mater. Lett.* **57**, 2432 (2003).

¹⁴P. R. Arya, P. Jha, G. N. Subbanna, and A. K. Ganguli, *Mater. Res. Bull.* **38**, 617 (2003).

¹⁵S. Bose and A. Banerjee, *J. Am. Ceram. Soc.* **87**, 487 (2004).

¹⁶A. Banerjee and S. Bose, *Chem. Mater.* **16**, 5610 (2004).

¹⁷H. P. Klug and L. E. Alexander, *X-ray Diffraction Procedures for Polycrystalline Materials* (Wiley, New York, 1974).

¹⁸V. Petkov, I.-K. Jeong, J. S. Chung, M. F. Thorpe, S. Kycia, and S. J. L. Billinge, *Phys. Rev. Lett.* **83**, 4089 (1999).

¹⁹Y. Waseda, *The Structure of Nanocrystalline Materials* (McGraw-Hill, New York, 1980).

²⁰T. Egami and S. J. L. Billinge, *Underneath the Bragg Peaks. Structural Analysis of Complex Materials* (Pergamon, Oxford, 2003).

²¹V. Petkov, *J. Appl. Crystallogr.* **22**, 387 (1989).

²²H. M. Rietveld, *J. Appl. Crystallogr.* **2**, 65 (1969).

²³*The Rietveld Method*, edited by R. A. Young (Oxford University Press, New York, 1996).

²⁴MAUD version 2.056, L. Lutterotti, <http://www.ing.unitn.it/~luttero/maud>.

²⁵E. Kakewaga, O. Matsunaga, T. Kato, and Y. Sasaki, *J. Am. Ceram. Soc.* **78**, 1071 (1995).

²⁶J. C. Fernandes, D. A. Hall, M. R. Cockburn, and G. N. Greaves, *Nucl. Instrum. Methods Phys. Res. B* **97**, 137 (1995).

²⁷M. Hammer, C. Monty, A. Endriss, and M. J. Hoffman, *J. Am. Ceram. Soc.* **81**, 721 (1998).

²⁸W. Cao and L. E. Cross, *Phys. Rev. B* **47**, 4825 (1993).

²⁹A. G. Souza Filho, K. C. V. Lima, A. P. Ayala, I. Guedes, P. T. C. Freire, J. Mendes Filho, E. B. Araújo, and J. A. Eiras, *Phys. Rev. B* **61**, 14283 (2000).

³⁰B. Noheda, D. E. Cox, G. Shirane, R. Guo, B. Jones, and L. E. Cross, *Phys. Rev. B* **63**, 014103 (2001).

³¹L. Bellaiche, A. Garcia, and D. Vanderbilt, *Phys. Rev. Lett.* **84**, 5427 (2000).

³²R. Guo, L. E. Cross, S.-E. Park, B. Noheda, D. E. Cox, and G. Shirane, *Phys. Rev. Lett.* **84**, 5423 (2000).

³³H. Fu and R. E. Cohen, *Nature (London)* **403**, 281 (2000).

³⁴W. Dmowski, T. Egami, L. Farber, and P. K. Davies, *AIP Conf. Proc.* **582**, 33 (2001).

³⁵M. Gateshki, S.-J. Hwang, D. H. Park, Y. Ren, and V. Petkov, *J. Phys. Chem. B* **108**, 14956 (2004); V. Petkov, M. Gateshki, M. Niederberger, and Y. Ren, *Chem. Mater.* **18**, 814 (2006).

³⁶V. Petkov, P. Y. Zavalij, S. Lutta, M. S. Whittingham, V. Parvanov, and S. Shastri, *Phys. Rev. B* **69**, 085410 (2004).

- ³⁷M. Gateshki, V. Petkov, G. Williams, S. K. Pradhan, and Y. Ren, *Phys. Rev. B* **71**, 224107 (2005).
- ³⁸V. Petkov, S. J. L. Billinge, S. D. Shastri, and B. Himmel, *Phys. Rev. Lett.* **85**, 3436 (2000).
- ³⁹It may be noted that the agreement factors achieved with the PDF analyses appear somewhat higher when compared to those usually resulted from the Rietveld analyses (see Table II) of conventional diffraction data in reciprocal space. This reflects the fact that the atomic PDF differs from the conventional XRD pattern being a quantity much more sensitive to the local atomic ordering in materials. As a result, R_w 's between 15 and 25% are common for PDF analyses. The inherently higher absolute value of the goodness-of-fit factors resulted from PDF-based analyses does not affect their functional purpose as a residuals quantity that must be minimized to find the best fit and as a quantity allowing to differentiate between competing structural models.
- ⁴⁰T. Proffen and S. J. L. Billinge, *J. Appl. Crystallogr.* **32**, 572 (1999).
- ⁴¹E. R. Camaro, E. Longo, E. R. Leite, and V. R. Mastelaro, *J. Solid State Chem.* **177**, 1994 (2004).
- ⁴²S. Ergun and S. R. Schehl, *Carbon* **11**, 127 (1973).
- ⁴³H. Zhang *et al.*, *Nature (London)* **424**, 1025 (2003).
- ⁴⁴R. J. Nelmes and W. F. Kuhs, *Solid State Commun.* **54**, 721 (1985).
- ⁴⁵D. Le Bellac, J. M. Kiat, P. Garnier, H. Moudden, Ph. Sciau, P. A. Buffat, and G. André, *Phys. Rev. B* **52**, 13184 (1995).
- ⁴⁶J. Moreau, P. Boher, and P. Garnier, *Mater. Res. Bull.* **24**, 1241 (1989).
- ⁴⁷K. Chhor, C. Pommier, P. Garnier, and L. Abello, *J. Phys. Chem. Solids* **52**, 895 (1991).
- ⁴⁸J.-R. Soh, H. M. Lee, and H.-S. Kwon, *CALPHAD: Comput. Coupling Phase Diagrams Thermochem.* **18**, 237 (1994).
- ⁴⁹A. D. Polli, F. F. Lange, and C. G. Levi, *J. Am. Ceram. Soc.* **83**, 873 (2000).
- ⁵⁰M. A. Subramanian, G. Aravamudan, and G. V. Subba Rao, *Prog. Solid State Chem.* **15**, 55 (1983).
- ⁵¹K. D. Budd, S. K. Dey, and D. A. Payne, *Br. Ceram. Proc.* **36**, 107 (1985).
- ⁵²C. E. Lakeman and D. A. Payne, *J. Am. Ceram. Soc.* **75**, 3091 (1992).
- ⁵³S. Hirano, T. Yogo, K. Kikuti, Y. Araki, M. Saitoh, and S. Ogashara, *J. Am. Ceram. Soc.* **75**, 2785 (1992).
- ⁵⁴S. P. Faure, P. Barboux, P. Gaucher, and J. Livage, *J. Mater. Chem.* **2**, 713 (1992).
- ⁵⁵H. Hirashima, E. Onishi, and M. Nakagawa, *J. Non-Cryst. Solids* **121**, 404 (1990).
- ⁵⁶J. Frantti, J. Lappalainen, S. Eriksson, V. Lantto, S. Nishio, M. Kakihana, S. Ivanov, and H. Rundlof, *Jpn. J. Appl. Phys., Part 1* **39**, 5697 (2002).
- ⁵⁷C. Cascales, J. A. Alonso, and I. Rasines, *J. Mater. Sci. Lett.* **5**, 675 (1986).
- ⁵⁸H. Fujishita and S. Katano, *Ferroelectrics* **237**, 209 (2000).